Swiveling Domain Mechanism in Pyruvate Phosphate Dikinase[†,‡]

Kap Lim,[§] Randy J. Read,[∥] Celia C. H. Chen,[§] Aleksandra Tempczyk,[§] Min Wei,[⊥] Dongmei Ye,[⊥] Chun Wu,[⊥] Debra Dunaway-Mariano,[⊥] and Osnat Herzberg*[,§]

Center for Advanced Research in Biotechnology, University of Maryland Biotechnology Institute, Rockville, Maryland 20850, Department of Haematology, Cambridge Institute for Medical Research, University of Cambridge, Cambridge, United Kingdom, and Department of Chemistry, University of New Mexico, Albuquerque, New Mexico

Received September 10, 2007; Revised Manuscript Received October 17, 2007

ABSTRACT: Pyruvate phosphate dikinase (PPDK) catalyzes the reversible conversion of phosphoenolpyruvate (PEP), AMP, and P_i to pyruvate and ATP. The enzyme contains two remotely located reaction centers: the nucleotide partial reaction takes place at the N-terminal domain, and the PEP/pyruvate partial reaction takes place at the C-terminal domain. A central domain, tethered to the N- and C-terminal domains by two closely associated linkers, contains a phosphorylatable histidine residue (His455). The molecular architecture suggests a swiveling domain mechanism that shuttles a phosphoryl group between the two reaction centers. In an early structure of PPDK from *Clostridium symbiosum*, the His445-containing domain (His domain) was positioned close to the nucleotide binding domain and did not contact the PEP/pyruvate-binding domain. Here, we present the crystal structure of a second conformational state of *C. symbiosum* PPDK with the His domain adjacent to the PEP-binding domain. The structure was obtained by producing a three-residue mutant protein (R219E/E271R/S262D) that introduces repulsion between the His and nucleotide-binding domains but preserves viable interactions with the PEP/pyruvate-binding domain. Accordingly, the mutant enzyme is competent in catalyzing the PEP/pyruvate half-reaction but the overall activity is abolished. The new structure confirms the swivel motion of the His domain. In addition, upon detachment from the His domain, the two nucleotide-binding subdomains undergo a hinge motion that opens the active-site cleft. A similar hinge motion is expected to accompany nucleotide binding (cleft closure) and release (cleft opening). A model of the coupled swivel and cleft opening motions was generated by interpolation between two end conformations, each with His455 positioned for phosphoryl group transfer from/to one of the substrates. The trajectory of the His domain avoids major clashes with the partner domains while preserving the association of the two linker segments.

The study reported here was undertaken to define a conformational state of pyruvate phosphate dikinase from *C. symbiosum* (*Cs*PPDK),[1] which, together with the conformation of the enzyme described earlier (*1*), provides experimental support for our proposed enzyme mechanism invoking a swiveling domain that shuttles a phosphoryl group between two remote reaction centers. PPDK catalyzes the interconversion of ATP, P_i, and pyruvate with AMP, PP_i, and phosphoenolpyruvate (PEP) in the presence of Mg^{2+} and K^+/Na^+ (*2*). The three-step reversible reaction proceeds via phosphoenzyme and pyrophosphoenzyme intermediates with a histidine residue serving as the phosphocarrier (*3*−*5*).

$$\text{Enz-His} + \text{PEP} \rightleftarrows \text{Enz-His}\sim\text{P} + \text{pyruvate}$$

$$\text{Enz-His}\sim\text{P} + \text{AMP}\cdot\text{PP}_i \rightleftarrows \text{Enz-His}\sim\text{P}-\text{P}\cdot\text{AMP} + \text{P}_i$$

$$\text{Enz-His}\sim\text{P}-\text{P}\cdot\text{AMP} \rightleftarrows \text{Enz-His} + \text{ATP}$$

PPDK has been found in bacteria, in C_4 and Crassulacean acid metabolism plants, and in parasites, but not in higher animal forms. In bacteria and parasites, PPDK functions in the direction of ATP synthesis, reminiscent of pyruvate kinase (*2*, *6*). In plants and in photosynthetic bacteria, PPDK functions in PEP formation, potentiating the rate of CO_2 fixation that takes place during photosynthesis (*7*). PPDK exhibits sequence homology to pyruvate phosphate synthase and to another enzyme that utilizes phosphotransfer from PEP to a histidine residues, enzyme I of the PEP:sugar phosphotransferase system (PTS) (*8*).

PPDK assembles into homodimers of ∼95 kDa subunit molecular mass. The monomer is composed of three domains and contains two distinct reaction centers. Each reaction

[†] Grant sponsors: NSF MCB9813271 (O.H.) and NIH RO1GM36260 (D.D.-M.).

[‡] Coordinates have been deposited in the Protein Data Bank (entry code 2R82). A movie showing the proposed conformational transition motion of PPDK may be watched or downloaded at http://carb.umbi.umd.edu/herzberg/research.

* Corresponding author: tel 240-314-6245; fax 240-314-6255; e-mail osnat@carb.nist.gov.

[§] University of Maryland Biotechnology Institute.

[∥] University of Cambridge.

[⊥] University of New Mexico.

[1] Abbreviations: PPDK, pyruvate phosphate dikinase; *Cs*PPDK, *Clostridium symbiosum* pyruvate phosphate dikinase; *Tb*PPDK, *Trypanosoma brucei* pyruvate phosphate dikinase; *Mz*PPDK, maize pyruvate phosphate dikinase; PEP, phosphoenolpyruvate; His domain, His455-containing domain; NBD1, subdomain 1 of nucleotide binding domain; NBD2, subdomain 2 of nucleotide binding domain; PCR, polymerase chain reaction; SDS−PAGE, sodium dodecyl sulfate−polyacrylamide gel electrophoresis; Hepes, *N*-(2-hydroxyethyl)piperazine-*N*′-ethanesulfonic acid; EDTA, ethylenediaminetetraacetic acid; DTT, dithiothreitol.

10.1021/bi701848w CCC: $37.00
Published on Web 12/04/2007

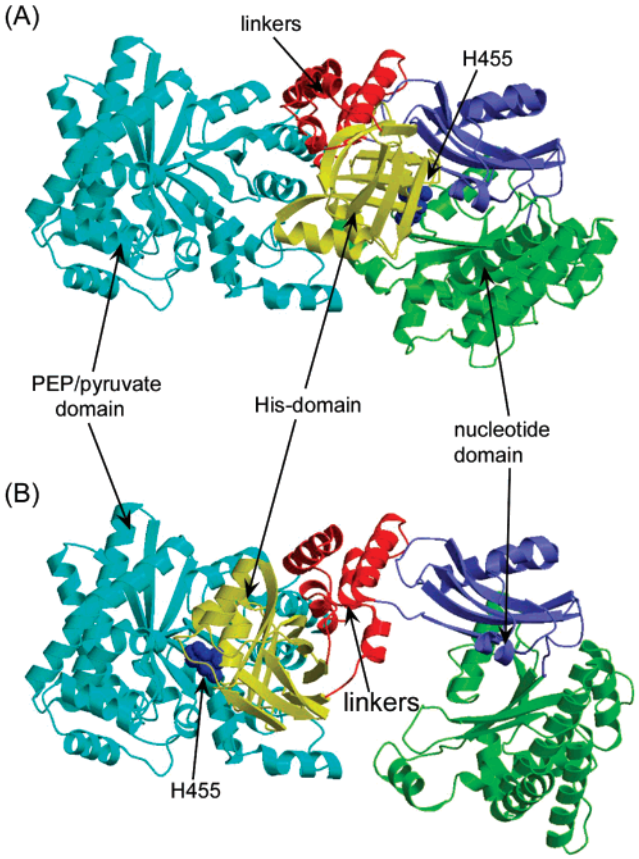

FIGURE 1: Two conformations of PPDK from *Clostridium symbiosum*. (A) *Cs*PPDK1 as defined in the 1.94 Å structure (*11*). The His domain (in yellow) is in close proximity to the nucleotide-binding domain (NBD1, green; NBD2, blue) and remotely located from the PEP/pyruvate-binding domain (cyan). The His domain is tethered to the partner domains by two closely associated linkers (red). The reactive histidine, His455, is depicted as a blue space-filling model. (B) *Cs*PPDK2 conformation. The His domain is close to the PEP/pyruvate-binding domain and remote from the nucleotide-binding domain. Coloring is the same as in panel A. All figures were generated with Molscript (*29*) and Raster3D (*30*, *31*).

center is responsible for half of the overall catalytic reaction (*9*). The N-terminal domain [adopting the so-called ATP grasp fold (*1*)] carries out the ATP/AMP reaction (nucleotide-binding domain), and the C-terminal domain [adopting an α/β barrel fold (*1*)] carries out the PEP/pyruvate reaction (PEP/pyruvate-binding domain). The phospho-carrier histidine residue (His455 in *Cs*PPDK) is located on a domain (His domain) that corresponds to the middle region of the polypeptide chain (*3*). The His domain shuttles the phosphate group between the two remotely located substrate binding sites (~45 Å apart). Its fold is unique to PPDK (*1*) and to the His domain of enzyme I (*10*). The first crystal structure of *Cs*PPDK was determined at 2.3 Å resolution (*1*) and later the resolution was extended to 1.94 Å resolution (*11*). In that structure, the His domain is tethered to the partner domains by two linkers that appear as an independent folding unit. The His and nucleotide-binding domains are closely associated and His455 faces the nucleotide binding site (Figure 1A). Modeling showed that if the His domain swivels around the two linker segments, it may be brought to interact with the PEP/pyruvate-binding domain such that His455 faces the PEP/pyruvate binding site. A 2.2 Å resolution structure of the enzyme that was obtained from crystals grown in the presence of Mg^{2+} and the inhibitor phosphonopyruvate, a PEP analogue, confirmed the location of the PEP binding site and identified the key residues involved (*11*). In both apo and phosphonopyruvate-bound structures, the nucleotide binding site is partially blocked by a loop, requiring that the nucleotide-binding domain undergoes a conformational transition upon binding of Mg^{2+}, ATP, and P_i.

Subsequent to the structure determination of *Cs*PPDK, the structure of PPDK from the African protozoan parasite *Trypanosoma brucei* (*Tb*PPDK) was determined at 3.0 Å resolution (*12*). The structure showed the same arrangement of the three domains, except that the two ATP grasp subdomains adopted a more open, substrate-accessible conformation.

Support for the swiveling domain mechanism was provided by the 2.3 Å resolution crystal structure determination of maize PPDK (*Mz*PPDK) (*13*), an enzyme that functions in the direction of PEP formation. In this structure, the His domain is oriented toward the PEP/pyruvate-binding domain but is not sufficiently close to the binding site for productive phosphoryl group transfer between PEP/pyruvate and the reactive histidine residue. While the collection of structures provides compelling evidence of the swiveling domain mechanism, so far the hypothesis has not been validated for the same PPDK molecule. This work provides direct experimental confirmation that the His domain of the same PPDK molecule can swivel around its linkers to adopt the two extreme conformational states. The new, second conformational state was obtained by introducing three mutations in the nucleotide-binding domain that repel the His domain and promote an alternative interaction with the PEP/pyruvate-binding domain. Kinetic analysis showed that the overall activity of the mutant enzyme was abolished; however, the mutant was competent in catalyzing the PEP/pyruvate half-reaction. This new structure sheds light on flexibility requirements in PPDK, an issue relevant to other enzymes that utilize the swiveling mechanism.

MATERIALS AND METHODS

Cloning, Expression, and Purification. The triple mutant PPDK (R219E/S262D/E271R) was produced by using the PCR-based strategy described previously (*14*). Mutagenic primers, 18−22 base pairs in length, were synthesized by Gibco BRL Life Science. *Bgl*II and *Bst*XI restriction sites were employed in mutant construction. The sequence of the mutant gene was confirmed by the Center for Agricultural Biotechnology at the University of Maryland. The mutant gene was expressed in *Escherichia coli* JM101 cells, and the protein product was purified to homogeneity (as determined by SDS−PAGE analysis) by the methods described previously (*14*).

Rapid-Quench Analysis of PPDK-Catalyzed Single-Turnover Reactions of [^{32}P]PEP. [^{32}P]PEP was synthesized and purified from [β-^{32}P]ATP according to the procedure described previously (*15*). [β-^{32}P]ATP (>1 Ci/mmol in specific activity) was custom-synthesized by NEN Life Science Products. The single-turnover reactions of 40 μM R219E/S262D/E271R PPDK, 5 μM [^{32}P]PEP, 2.5 mM $MgCl_2$, and 10 mM NH_4Cl in 50 mM K^+ Hepes (pH 7.0, 25 °C) were carried out in a rapid-quench instrument from KinTek Instruments. Reactions were initiated by mixing 32

Table 1: X-ray Data Processing and Refinement Statistics

Data Collection	
space group	$C222_1$
cell dimensions (Å)	90.4, 125.1, 184.0
wavelength (Å)	1.5418
resolution (Å)	20−3.6 (3.8−3.6)[a]
no. of unique reflections	11 406
completeness, %	91.0 (76.5)[a]
redundancy	2.5
R_{merge}[b]	0.155 (0.331)[a]
$\langle I/\sigma(I)\rangle$	6.1 (2.5)[a]
Refinement	
R_{work}[b]	0.265
R_{free}[b]	0.325
rmsd from ideal geometry	
bond length (Å)	0.01
bond angle (deg)	1.2

[a] Statistics for the highest-resolution shell are given in parentheses. [b] $R_{merge} = \Sigma_{hkl}\,[(\Sigma_j\,|I_j - \langle I\rangle|)/\Sigma_j\,|I_j|\,]$; $R_{work} = \Sigma_{hkl}\,||F_o| - |F_c||/\Sigma_{hkl}\,|F_o|$, where F_o and F_c are the observed and calculated structure factors, respectively. R_{free} is computed for 9% randomly selected reflections omitted from the refinement.

μL of buffered enzyme/cofactors with 32 μL of buffered substrate and then terminated at varying conversion with 182 μL of 0.6 M HCl. The protein was precipitated from quenched solutions by vigorous mixing with CCl_4 and separated by centrifugation. The protein pellet (dissolved in 500 μL of boiling 10 N H_2SO_4) and supernatant were analyzed for ^{32}P radioactivity by scintillation counting. The percent conversion was deduced from the ratio of unconsumed [^{32}P]PEP (in the supernatant) and produced E-P (in protein pellet) in each reaction. The product (E-P) formation (micromolar concentration) was calculated by multiplying the initial substrate concentration by the percent conversion. Time course data of product formation were fit to a single-exponential equation (eq 1) with the KaleidaGraph program to yield the rate constants for the single-turnover reactions.

$$[B]_t = [B]_\infty(1 - \exp(k_{obs}t)) \quad (1)$$

where $[B]_t$ is the product (E-P) concentration at time t, $[B]_\infty$ is the product concentration at equilibrium, and k_{obs} is the observed rate constant for the reaction.

Crystallization and Diffraction Data Collection. Crystals were obtained at 30 °C in hanging drops by the vapor diffusion method. The protein solution (28 mg/mL) contained 20 mM imidazole (pH 6.5), 0.1 mM EDTA, 100 mM KCl, and 1 mM DTT. The reservoir solution contained 50% saturated ammonium sulfate and 0.1 M Na^+Hepes (pH 7.0). The hanging drops consisted of equal volumes of protein solution and reservoir solution. Diffraction data were collected at room temperature with Cu Kα X-rays generated by a Siemens rotating anode, which was monochromated with Harvard mirrors and equipped with a Mar345 imaging plate detector. Data were processed with the HKL programs suite (*16*). The diffraction resolution limit was 3.6 Å (Table 1). The crystals belong to space group $C222_1$, the asymmetric unit contains one PPDK molecule, and the solvent comprises 53% of the unit cell.

Structure Determination. The structure was determined by molecular replacement. The computations were carried out with the program Phaser (*17*, *18*) and autonomous domains and subdomains of the *Cs*PPDK structure determined at 1.94 Å resolution served as search models (*11*). The structure was refined at 3.6 Å resolution with the CNS program (*19*), followed by REFMAC 5.0 (*20*). Structure modifications in accordance with the electron density map were made with the O interactive graphics program (*21*). A single temperature factor was refined for each of the four domains of *Cs*PPDK and then for each amino acid residue. The application of single-residue temperature factors was assessed to be appropriate because it led to significant reduction in the free-*R* value. Final refinement cycles were performed with the REFMAC program, employing TLS parameters (four domains) to model anisotropic displacements.

RESULTS AND DISCUSSION

Mutant Design. In the following discussion, the *Cs*PPDK conformation observed in all earlier crystal structures is referred to as *Cs*PPDK1 [see for example the PDB entry code of the most accurate structure determined at 1.94 Å resolution, 1kbl (*11*), Figure 1A], whereas the structure reported here will be referred to as *Cs*PPDK2. Following a number of failed attempts to obtain a structure of *Cs*PPDK2, a strategy that employed site-directed mutagenesis proved successful.

Replacement of three residues in the nucleotide binding domain (R219E/S262D/ E271R) was expected to result in repulsion between the His domain and the nucleotide-binding domain. Inspection of the environment of these residues showed that the replacement R219E could potentially introduce electrostatic repulsion between the newly introduced carboxylate group and the backbone carbonyl groups of the His domain's Pro433 and Glu434, as well as the carboxylate groups of Glu434 and Glu437 (Figure 2A). For a S262D replacement in the context of the *Cs*PPDK1 conformation, the newly introduced carboxylate group would be oriented toward the carbonyl groups of Pro397 and Ala398, again forming unfavorable electrostatic interactions (Figure 2B). Finally, the mutation E271R would eliminate the carboxylate group interaction with two main-chain amide groups on the His domain, Met452 and Thr453, and would instead introduce both electrostatic and steric repulsion (Figure 2C). All three mutated residues are located outside the nucleotide binding cleft. By modification of the nucleotide-binding domain residues while the amino acid sequence of the His domain was preserved, the potential interactions between the His domain and the PEP/pyruvate-binding domain were not affected. Indeed, *Cs*PPDK2 exhibits a conformation in which the His domain sways away from the nucleotide-binding domain toward the PEP/pyruvate-binding domain (Figure 1B). The kinetic characterization reported below confirmed the preservation of productive interaction between the His and PEP/pyruvate-binding domains. In contrast, when complementary mutations were made on the His domain (E434A/E437A and T453A, the positions of which are shown in Figure 1, panels A and C, respectively), both nucleotide and PEP partial reactions were impaired (*22*).

Enzyme Kinetics. The catalytic activity of the triple mutant (40 μM) in the conversion of 0.5 mM AMP, 1.0 mM PP_i, and 0.5 mM PEP to ATP, PP_i, and PEP in 20 mM imidazole (pH 6.8 and 25 °C) containing 5 mM $MgCl_2$ and 40 mM NH_4Cl, was too low to detect by the lactate dehydrogenase/

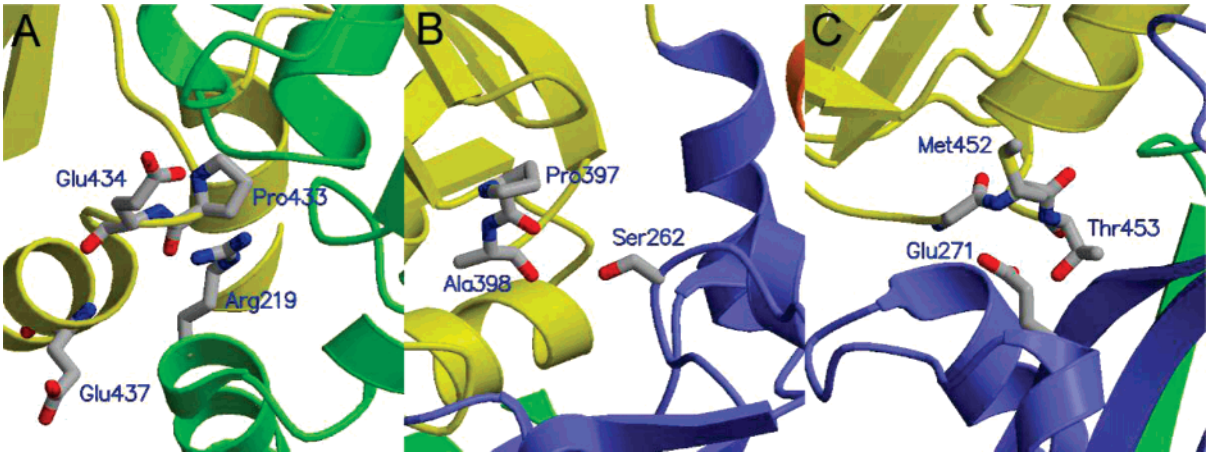

FIGURE 2: Environments of the three nucleotide-binding domain residues that were mutated to generate a molecule that adopts the *Cs*PPDK2 conformation: (A) Arg219, (B) S262, and (C) Glu271. Backbone coloring scheme is as in Figure 1. Atom colors: gray, carbon; blue, nitrogen; red, oxygen.

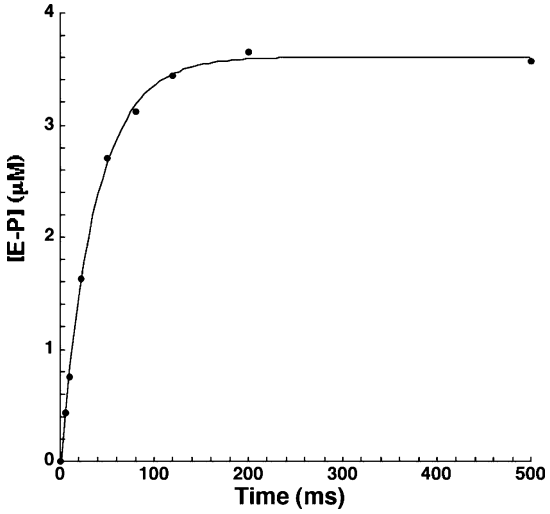

FIGURE 3: Time course for [^{32}P]E-P formation in the single-turnover reaction of 40 μM R219E/E271R/S261D, 5 μM [^{32}P]PEP, 2.5 mM $MgCl_2$, and 10 mM NH_4Cl in 50 mM K^+HEPES (pH 7.0, 25 °C). The data were fitted with eq 1 (see Materials and Methods).

NADH-coupled spectrophotometric assay. Likewise, the rate of R219E/S262D/E271R PPDK (40 μM) catalyzed conversion of 2 mM [^{14}C]ATP, 5 mM P_i, and 5 mM pyruvate in 50 mM K^+Hepes containing 5 mM $MgCl_2$ and 40 mM NH_4-Cl (pH 7.0, and 25 °C) to [^{14}C]AMP, PP_i, and PEP (equilibrium-driven with inorganic pyrophosphatase to hydrolyze PP_i; monitored by HPLC separation of the reaction mixture) was too low to detect. On the other hand, PEP phosphorylation of the R219E/S262D/E271R PPDK catalytic His455, determined by transient kinetic methods, occurred at a rate comparable to that observed with wild-type PPDK. The single-time-course data shown in Figure 3 were fitted with a first-order rate equation to define a $k_{obs} = 30\ s^{-1}$ compared to the $k_{obs} = 40\ s^{-1}$ measured for the wild-type enzyme under the same conditions. Thus, the triple mutant is unable to catalyze the partial reaction at the N-terminal domain active site but retains full catalytic efficiency toward the partial reaction at the C-terminal domain. This result is consistent with impaired docking of the N-terminal domain and the His domain.

Structure Determination. Structure determination by molecular replacement was not straightforward, perhaps because of the anisotropic nature of the diffraction. The position of the PEP/pyruvate-binding domain was easily identified by the *AMoRe* molecular replacement program (*23*). However, in our hands, the remaining two domains were not resolved despite various searches that employed models of subdomains expected to undergo rigid-body motions. Ultimately, the molecular replacement solution was obtained by use of the program Phaser (*17*, *18*) as follows. The PPDK molecule was divided into six domains, each forming an entity that appeared to form a compact autonomous folding unit. The nucleotide-binding domain contained three such units: the first folding unit spanned residues 2−111 together with 197−243, the second folding unit spanned residues 112−196 (a helix bundle), and the third folding unit spanned residues 244−341. The first two folding units form the ATP grasp subdomain that is abbreviated NBD1 in the following discussion, and the third folding unit corresponds to the second ATP grasp subdomain that is abbreviated NBD2. The cleft between the two subdomains defines the nucleotide binding site (*1*, *14*, *24*, *25*). A fourth fragment used in the molecular replacement included residues 342−377 spanning the linker between the nucleotide-binding domain and the His domain. The molecular replacement search model for the His domain spanned residues 378−517 and the PEP/pyruvate-binding domain search model spanned residues 518−873. The position of the PEP/pyruvate-binding domain was easily resolved with Phaser as it was with *AMoRe*. Next, with the already identified PEP/pyruvate-binding domain included as a partial model, the two nucleotide-binding subdomains were positioned in the cell. The position of the His domain remained elusive and was resolved only after the anisotropy correction in Phaser was improved. For this search, the fixed partial model included all previously resolved fragments. Analysis of the principal components of the anisotropic part of the temperature factor affecting observed amplitudes showed a difference of approximately 30 Å^2 between the weakest (0*k*0) and strongest (*h*00) diffraction directions. The anisotropy may be attributed to crystal packing; the molecules pack such that the tight dimer interface (mediated by the PEP/pyruvate-binding domain) is along the *a* unit cell axis, dimers pack to form continuous rows along the *c* unit cell axis, and the least extensive intermolecular interactions occur along the *b* unit cell axis.

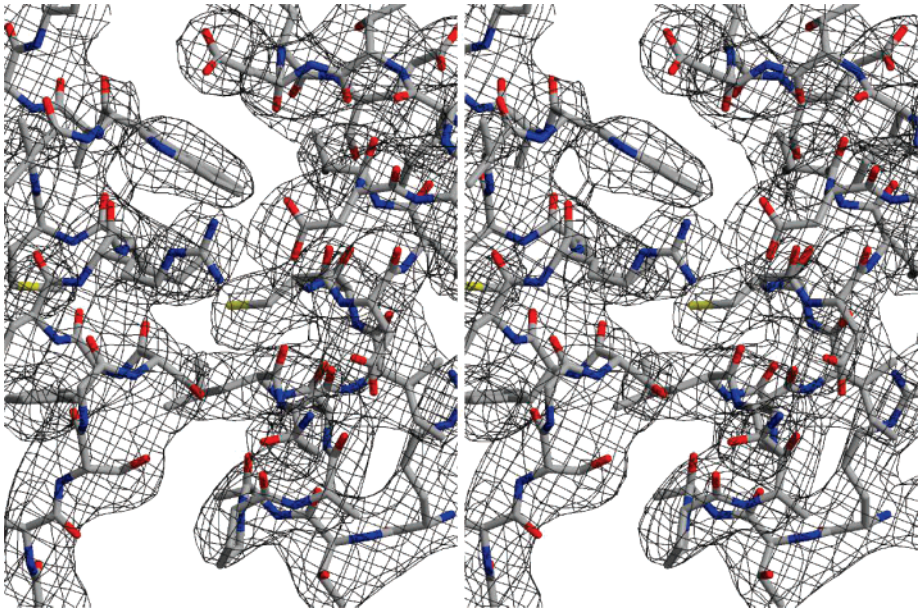

FIGURE 4: Stereoscopic representation of the electron density associated with a region of the interdomain linkers (residues 341−363 and 516−530 on the left and right sides of the image, respectively). The SIGMAA-weighted $2F_o - F_c$ map is shown contoured at 1σ level. Atom colors: carbon, gray; oxygen, red; nitrogen, blue.

Refinement of the *Cs*PPDK2 structure at 3.6 Å led to *R* values that are well within the range observed for structures refined at such limited resolution and available in the PDB. The quality of the electron density map is demonstrated in Figure 4. Consistent with the stereochemistry of the model used in the search (refined at a much higher resolution of 1.94 Å), all backbone torsion angles are within the allowed region of the Ramachandran plot. Surprisingly, and despite the low resolution of the data, clear electron density consistent with two sulfate ions was evident. These are located in the PEP/pyruvate-binding site, close to the His domain, and are surrounded by arginine residues.

Molecular Conformation. With one molecule in the asymmetric unit, the dimer interface is formed across a crystallographic 2-fold symmetry axis. As in *Cs*PPDK1, which was crystallized in a different space group (*P*2), interactions between subunits are mediated by the PEP/pyruvate-binding domain. Within the resolution limit of the diffraction data, the PEP/pyruvate-binding domain has not changed compared with *Cs*PPDK1, and the dimer interface remained unperturbed. This conclusion was confirmed computationally by superposing one PEP/pyruvate-binding domain of *Cs*PPDK1 and *Cs*PPDK2, which places the respective partner domain in equivalent position with root-mean-square deviation (rmsd) value for Cα atoms of 0.6 Å. The position of the partner domain was further optimized by allowing independent movement of the second domain, yielding an rmsd value of 0.2 Å following a slight rotation of 1.4°.

The conformations of NBD2 and the His domain are also very similar in the two structures of *Cs*PPDK. Superposition of the Cα atoms of each of these domains (excluding the two His domain linkers, Figure 1) resulted in rmsd values lower than 1 Å. In contrast, the rmsd value is larger for NBD1, at 1.9 Å. The main changes occur in two NBD1 loop regions, residues 217−232 and 98−103. In *Cs*PPDK1, these loops are constrained by contacts with a loop encompassing residues 793−802 on the PEP/pyruvate-binding domain. Unlike *Cs*PPDK1, NBD1 of *Cs*PPDK2 does not interact at all with the PEP/pyruvate-binding domain (Figure 1), enabling the two NBD1 loops (residues 217−232 and 98−103) to adopt new, more extended, conformations. The change in relative orientation of NBD1 and NBD2 results in a more open nucleotide binding cleft (Figure 1), similarly to the arrangement seen in *Tb*PPDK (*12*). The cleft opening is accompanied by conformational adjustment of the NBD1 loop residues 32−36.

We previously described a model of ATP bound to PPDK based on ADP binding to another enzyme that contains an ATP grasp fold, D-Ala-D-Ala ligase (*1*). The model showed that the nucleotide's ribose site was blocked in *Cs*PPDK1 by a NBD2 loop (residues 273−288). The conformation of this loop remains unaltered in *Cs*PPDK2; however, the ribose site is now accessible because of the shift that NBD1 undergoes relative to NBD2. One would expect that the two subdomains undergo closure upon nucleotide binding, but the closure must be accompanied by some local adjustments that allow nucleotide access to the binding site.

The two conformational states of *Cs*PPDK reveal that the His domain rotates as a rigid body, and the rotation is facilitated by torsions around backbone bonds of segments that tether the domain to the nucleotide- and PEP/pyruvate-binding domains (Figures 1 and 5). Following Nakanishi et al. (*13*), the program DynDom (*26*) was used to analyze the quasi-rigid-body domain motion, yielding an effective hinge axis (see Table 1 for the definition of effective hinge axis). This analysis yielded a 111° rotation of the His domain along an axis approximately parallel to linker segments that adopt extended conformations (residues 373−382 and 507−520) and passing between the two. The effective hinge axis has a translation component of −1.8 Å. The swivel-like motion results in a 38 Å displacement of His455 so that it faces the nucleotide-binding domain at one extreme (as in *Cs*PPDK1) and the PEP/pyruvate-binding domain at the other extreme

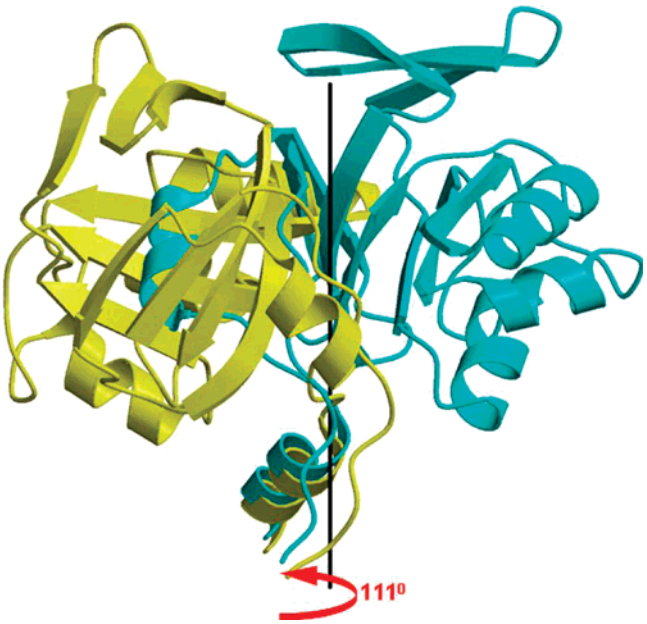

FIGURE 5: Swivel motion of the His domain. The location of the His domain was derived by superposing the PEP/pyruvate-binding domain of the *Cs*PPDK1 and *Cs*PPDK2 structures (Figure 1). The effective hinge axis calculated by DynDom (*26*) is indicated by the black line. The domain colored gold corresponds to *Cs*PPDK1, and that in cyan corresponds to *Cs*PPDK2.

(as in *Cs*PPDK2). The linker segments that exhibit the largest changes in backbone torsion angles span residues 378−382 and 512−518.

Bacterial, Trypanosome, and Maize PPDK Conformations The DynDom algorithm was used to compare domain orientations in the bacterial, trypanosome, and maize PPDK structures, omitting the automated domain assignment. Instead, the molecules were divided into four domains (NBD1, NBD2, His domain, and PEP/pyruvate domain), and the PEP/pyruvate domain of *Cs*PPDK1 served as the reference structure for the comparisons. Domain assignment by structure inspection provided a common framework for all PPDK structures, in contrast to the automatic domain assignment, which yielded different domain definitions of the different enzymes. Only domain core residues common to all three proteins (comprising approximately 80% of the residues of each domain) were included to prevent spurious results arising from sequence differences of proteins from different sources that are manifested structurally. By defining domains in this manner, the PEP/pyruvate-binding domains of the various structures were superposed with Cα atom rmsd values of 0.2 Å for *Cs*PPDK2 and 0.8 Å for both *Mz*PPDK (PDB entry code 1VBH) and *Tb*PPDK (PDB entry code 1H6Z) (Table 2). The analysis shows that NBD2 exhibits a small rigid-body movement relative to the PEP/pyruvate domain whereas movements of the His domain and NBD1 are much more extensive. The analysis summarized in Table 2 substantiates the notion of quasi-rigid-body motions of PPDK domains.

The rotation around the effective hinge axis of the *Cs*PPDK His domain remains the same as that obtained from the automated DynDom analysis (111°), but the translational component along the rotation axis is reduced from −1.8 to −0.8 Å. This rotation angle is larger than the corresponding rotation calculated for *Mz*PPDK (87°), as *Cs*PPDK2's His domain is closer to the orientation required for phosphotransfer compared with the *Mz*PPDK His domain; the positions of the Cα atoms of the reactive histidines in *Cs*PPDK2 and *Mz*PPDK are respectively 11 and 16 Å away from the position that would station the imidazole ring for productive phosphotransfer. These distances were calculated relative to a model (generated as described in the next section) of the *Cs*PPDK that enables the phosphotransfer reaction to occur.

Compared with *Cs*PPDK1, the opening of the active-site clefts of the nucleotide binding domains of *Cs*PPDK2, *Tb*PPDK, and *Mz*PPDK occur through a large rotation of the NBD1 subdomain (42−43°) and a smaller rotation of the NBD2 subdomain (7−13°) (Table 2). The effective hinge axis that describes the NBD2 motion is nearly perpendicular to the polypeptide segment that links the two subdomains (residues 241−245 in *Cs*PPDK; Figure 6). The small rigid-body rotation of NBD2 can be described by a hinge motion with the axis approximately perpendicular to residues 357−362 within the segment linking NBD2 and the His domain (not shown).

As with *Cs*PPDK1, the His domain of *Tb*PPDK interacts with the nucleotide binding domain; however, the *Tb*PPDK nucleotide-binding domain adopts an open conformation. Consequently, the His domain in *Tb*PPDK interacts exclusively with NBD2, whereas the closed conformation of the *Cs*PPDK1 nucleotide-binding domain leads to the His domain interacting with both NBD1 and NBD2.

Phosphoryl Group Transfer between PEP and His455. The His domains of *Cs*PPDK2 and of *Mz*PPDK are oriented away from their respective nucleotide-binding domains toward the PEP/pyruvate-binding domains, yet in both structures the domains are positioned too far for phosphoryl group transfer. The *Mz*PPDK crystals soaked with Mg^{2+}-PEP revealed the phosphoryl phosphorus atom 16 Å away from the Cα atom of the reactive histidine residue (*13*), and in fact the His domain and the PEP/pyruvate-binding domain in *Mz*PPDK do not form interdomain contacts. The His domain and the PEP/pyruvate-binding domain in *Cs*PPDK2 are positioned ∼5 Å closer together, yet this is also a loose association involving only a few van der Waals contacts. The Cα atom of His455 is stationed 11 Å away from the position of the PEP's phosphorus atom [inferred from the *Cs*PPDK structure in complex with Mg^{2+}-phosphonopyruvate (*11*)] and the side-chain conformation is inaccessible for phosphoryl group transfer.

To facilitate phosphoryl group transfer, the swivel angle of the His domain must be 103° rather than 111° and the His455 side chain χ1 dihedral angle must be rotated by approximately 120°. The model is consistent with stereochemical studies in solution (*27*), which invoke the associative mechanism's in-line transfer of the phosphoryl group. At the transition state, the phosphorus is pentagonally coordinated with trigonal bipyramidal geometry and the donor and acceptor groups are at the apical positions. The structure of phosphorylated enzyme I from *E. coli*, determined in the presence of Mg^{2+} and the inhibitor oxalate (an analogue of pyruvate enolate) guided the model building (*10*). Interestingly, one of the sulfate ions identified in the electron density map is located in the expected site of the phosphoryl group, and this sulfate site is also observed in the apo *Cs*PPDK1 and *Mz*PPDK structures.

Table 2: Superposition and Effective Hinge Axes of Core Cα Atoms of PPDK Domains[a]

		*Cs*PPDK2		*Mz*PPDK		*Tb*PPDK	
domain	no. of residues fitted	rmsd	effective hinge axis	rmsd	effective hinge axis	rmsd	effective hinge axis
PEP/pyruvate	300 (84%)	0.2 Å		0.8 Å		0.8 Å	
His domain	107 (78%)	0.2 Å	111°, −0.8 Å	0.8 Å	87°, 1.8 Å	0.8 Å	14°, −0.5 Å
NBD1	191 (79%)	1.3 Å	42°, −1.2 Å	1.6 Å	43°, −0.9 Å	1.4 Å	43°, −2.3 Å
NBD2	108 (79%)	0.5 Å	7°, 0.3 Å	0.9 Å	13°, 1.2 Å	0.6 Å	12°, 0.5 Å

[a] *Cs*PPDK1 was used as the reference molecule. The PEP/pyruvate domain of each structure was first superimposed on that of *Cs*PPDK1, and pairwise analysis of each of the remaining domains was then carried out. The effective hinge axis is defined as an interdomain screw axis that passes within 3 Å of the Cα atom of any of the interdomain residues involved in the interdomain motion (*26*).

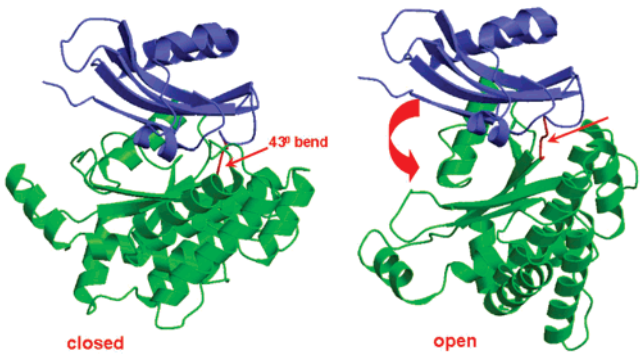

FIGURE 6: Opening and closure of the nucleotide-binding domain. The two subdomains are colored as in Figure 1, and the short peptide linking them is highlighted in red. The hinge motion is around an axis perpendicular to this peptide linker.

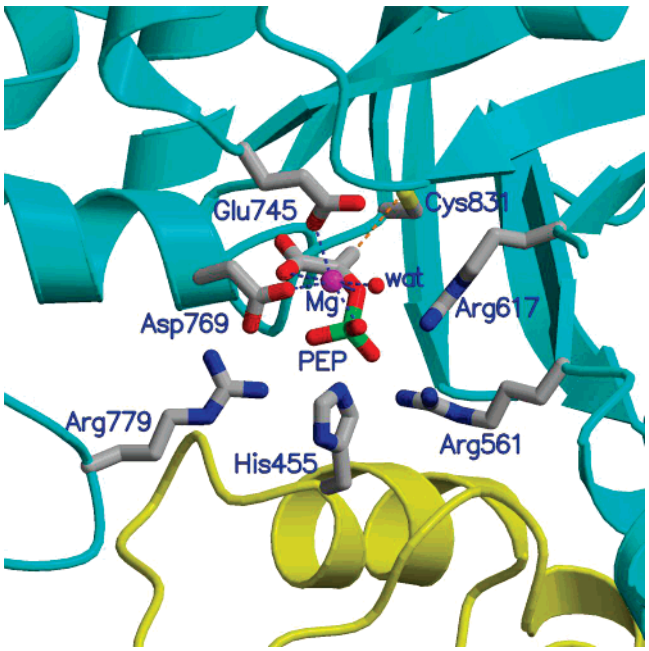

FIGURE 7: Model of His455 positioned in line for accepting the phosphoryl group from PEP. The model was generated as described in the text and is consistent with the crystal structure of phosphorylated enzyme I (*10*). Domain color scheme is as in Figure 1. Atom colors: gray, carbon; blue, nitrogen; red, oxygen; yellow, sulfur; green, phosphorus.

The model exhibits only a few steric clashes, primarily between side chains, which are readily relieved by energy minimization. Adjustments were made to the side chains of Arg561, Arg617, Arg665, and Arg779, invariant in all PPDK sequences, to position their guanidinium groups in proximity with the phosphoryl group (Figure 7). Support for the interaction of three arginine residues, Arg561, Arg617, and

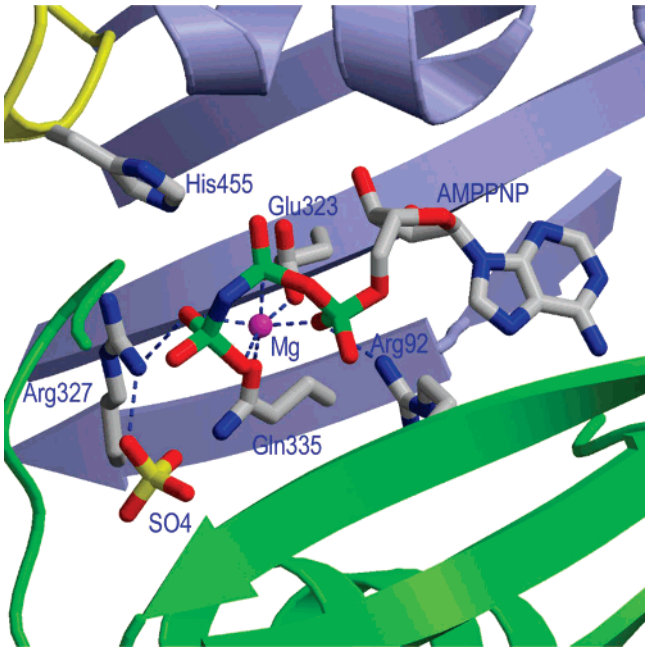

FIGURE 8: AMP-PNP bound in the nucleotide-binding cleft. By analogy, His455 is positioned in line for accepting the β-phosphate from ATP. By analogy to the SO_4 ion, PO_4^{3-} is positioned in line to accept the γ-phosphate of ATP. Domain color scheme is as in Figure 1. Atom colors: gray, carbon; blue, nitrogen; red, oxygen; yellow, sulfur; green, phosphorus.

Arg665, is provided by the structure of *Cs*PPDK in complex with phosphonopyruvate [cocrystallized with the His domain interacting with the nucleotide-binding domain (*11*)] and by the structure of *Mz*PPDK soaked with PEP [the His domain remains in the nonproductive conformation (*13*)]. The conformation of the fourth arginine, Arg779, must change when the His domain adopts the phosphotransfer productive state; otherwise the Arg779 side chain penetrates the His domain. The catalytic properties of site-directed mutants substantiate the model; the replacement of Arg561 by a leucine or a lysine and Arg617 by a lysine resulted in enzymes that failed to catalyze the PEP partial reaction (*11*, *28*). Moreover, all four arginine residues are invariant in both PPDK and enzyme I (*8*), and the structure of enzyme I in the phosphorylated state revealed the same arginine interactions (*10*). Similarly, the interaction of Asn768 with the phosphoryl group and that of the catalytic Cys831 with the pyruvyl C3 atom have their counterparts in enzyme I.

Swiveling Domain Mechanism. The two observed conformational states of *Cs*PPDK support a molecular machine that couples the three partial chemical reactions with a swiveling motion of the His domain and with closure and opening of the nucleotide-binding cleft. A model of these coupled motions was generated by interpolating between two end

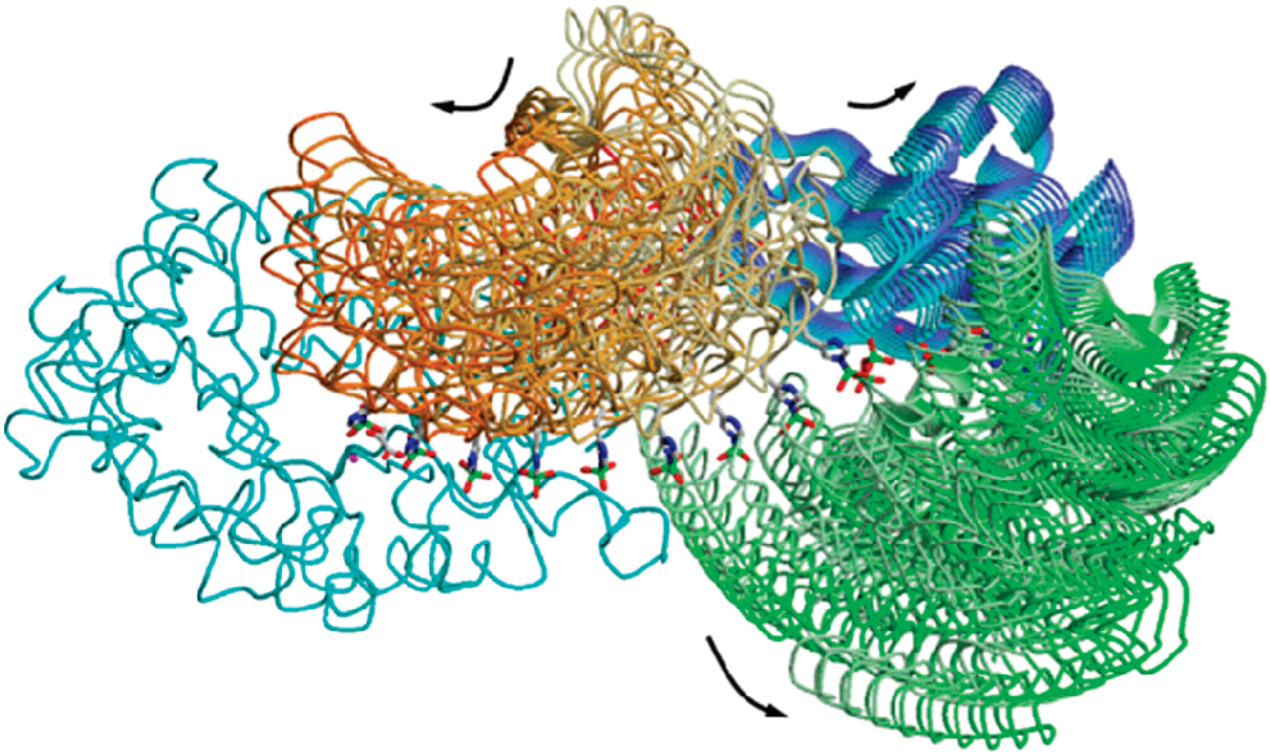

FIGURE 9: Proposed trajectory of the His domain and nucleotide-binding domain along the PPDK reaction pathway. Interpolations between the two end conformations were calculated as described in the text. Every tenth interpolation point is plotted in the figure. The PEP/pyruvate binding domain is colored cyan. The His domain color is changed from gray to brown along the trajectory. NBD1 color is changed from light green to dark green and NBD2 color is changed from light blue to dark blue along the trajectory. Phosphorylated His455 is depicted as a stick model.

states: one state corresponds to the structure of *Cs*PPDK bound to Mg^{2+} and AMP-PNP, which represents the state prior to the nucleotide and P_i partial reactions (Figure 8; K.L., D.D.-M., and O.H., to be published), and the second state corresponds to the model of the enzyme prior to the PEP partial reaction that was described above (Figure 7). Rotation around the effective hinge axis as calculated by the DynDom program resulted in substantial clashes of the His domain along its trajectory because the axis was defined by considering only the two end states. To avoid these clashes, the effective hinge axis was tilted by 20°. A total of 90 interpolation points were generated and each was energy-minimized to relieve minor clashes, yielding a trajectory that is illustrated in Figure 9.

It should be emphasized that in generating the conformational transition model, the intention is to demonstrate the feasibility of the swiveling motion and not to imply that this is the true detailed reaction pathway. Moreover, the model is not expected to reproduce the catalytic rates because it ignores nonproductive fluctuations.

The following conclusions are evident from the model. First, the His domain sways between the two extreme states as a rigid body while the fold integrity of the linkers is maintained, consistent with the observation that the linkers' association persists in the two experimental end conformational states of *Cs*PPDK (Figure 1). Second, in principle the same end point may be reached by the 103° rotation or by the counter rotation corresponding to (360° − 103°). However, the counter-rotation causes entanglement of the two linkers and substantial domain−domain interpenetration. Hence, assuming that no gross unfolding takes place, only one direction of the rotation is possible (anticlockwise, for a swivel from the nucleotide-binding domain to the PEP/pyruvate-binding domain depicted in Figure 9). Along this

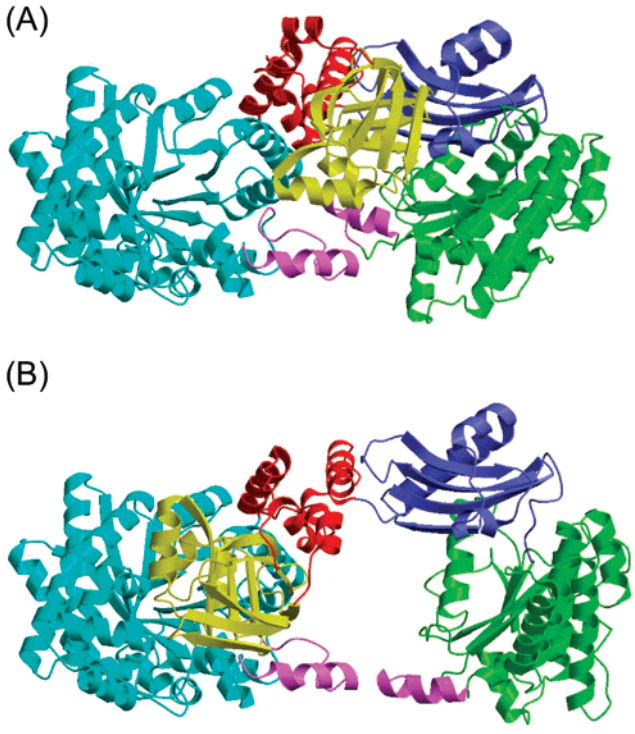

FIGURE 10: Two conformational states of PPDK, highlighting in magenta the helices that mediate interactions between the nucleotide- and PEP/pyruvate-binding domains in *Cs*PPDK1 (A) and their positions in *Cs*PPDK2 (B).

trajectory, the His domain traverses two helices (highlighted in magenta in Figure 10), mediating an interaction between the nucleotide- and PEP/pyruvate-binding domains in *Cs*PPDK1 and splaying apart when the nucleotide-binding domain adopts the open conformation observed in *Cs*PPDK2. Each of these helices is appended to the core fold of its respective domain (viz. the ATP grasp and α/β barrel). In the nucleotide-bound state, the resulting continuous surface shields the high-energy phospho∼His455 from solvent throughout the conformational transition, thus preventing an undesired hydrolysis of the phosphoryl group.

Finally, the time scale of the conformational change has not been yet determined but the turnover rate of the overall PPDK reaction sets an upper limit [$\sim$25 s^{-1} (*22*)]. As the swivel motion is rather extensive, it would be interesting to know whether the conformational transition constitutes the rate-limiting step of the reaction and whether this transition is diffusion-controlled or driven by specific molecular interactions.

REFERENCES

1. Herzberg, O., Chen, C. C. H., Kapadia, G., McGuire, M., Carroll, L. J., Noh, S. J., and Dunaway-Mariano, D. (1996) Swiveling-domain mechanism for enzymatic phosphotransfer between remote reaction sites, *Proc. Natl. Acad. Sci. U.S.A. 93*, 2652−2657.
2. Evans, H. J., and Wood, H. G. (1968) The mechanism of the pyruvate, phosphate dikinase reaction, *Proc. Natl. Acad. Sci. U.S.A. 61*, 1448−1453.
3. Goss, N. H., Evans, C. T., and Wood, H. G. (1980) Pyruvate phosphate dikinase: sequence of the histidyl peptide, the pyrophosphoryl and phosphoryl carrier, *Biochemistry 19*, 5805−5809.
4. Milner, Y., Michaels, G., and Wood, H. G. (1978) Pyruvate, phosphate dikinase of *Bacteroides symbiosus*. Catalysis of partial reactions and formation of phosphoryl and pyrophosphoryl forms of the enzyme, *J. Biol. Chem. 253*, 878−883.
5. Spronk, A. M., Yoshida, H., and Wood, H. G. (1976) Isolation of 3-phosphohistidine from phosphorylated pyruvate, phosphate dikinase, *Proc. Natl. Acad. Sci. U.S.A. 73*, 4415−4419.
6. Reeves, R. E. (1968) A new enzyme with the glycolytic function of pyruvate kinase, *J. Biol. Chem. 243*, 3202−3204.
7. Hatch, M. D., and Slack, C. R. (1968) A new enzyme for the interconversion of pyruvate and phosphopyruvate and its role in the C4 dicarboxylic acid pathway of photosynthesis, *Biochem. J. 106*, 141−146.
8. Pocalyko, D. J., Carroll, L. J., Martin, B. M., Babbitt, P. C., and Dunaway-Mariano, D. (1990) Analysis of sequence homologies in plant and bacterial pyruvate phosphate dikinase, enzyme I of the bacterial phosphoenolpyruvate: sugar phosphotransferase and other PEP-utilizing enzymes. Identification of potential catalytic and regulatory motifs, *Biochemistry 29*, 10757−10765.
9. Xu, Y., McGuire, M., Dunaway-Mariano, D., and Martin, B. M. (1995) Separate site catalysis by pyruvate phosphate dikinase as revealed by deletion mutants, *Biochemistry 34*, 2195−2202.
10. Teplyakov, A., Lim, K., Zhu, P. P., Kapadia, G., Chen, C. C., Schwartz, J., Howard, A., Reddy, P. T., Peterkofsky, A., and Herzberg, O. (2006) Structure of phosphorylated enzyme I, the phosphoenolpyruvate:sugar phosphotransferase system sugar translocation signal protein, *Proc. Natl. Acad. Sci. U.S.A. 103*, 16218−16223.
11. Herzberg, O., Chen, C. C. H., Liu, S., Tempczyk, A., Howard, A., Wei, M., Ye, D., and Dunaway-Mariano, D. (2002) Pyruvate site of pyruvate phosphate dikinase: crystal structure of the enzyme−phosphonopyruvate complex, and mutant analysis, *Biochemistry 41*, 780−787.
12. Cosenza, L. W., Bringaud, F., Baltz, T., and Vellieux, F. M. D. (2002) The 3 Å resolution crystal structure of glycosomal pyruvate phosphate dikinase from *Trypanosoma brucei*, *J. Mol. Biol. 318*, 1417−1432.
13. Nakanishi, T., Nakatsu, T., Matsuoka, M., Sakata, K., and Kato, H. (2005) Crystal structures of pyruvate phosphate dikinase from maize revealed an alternative conformation in the swiveling-domain motion, *Biochemistry 44*, 1136−1144.
14. McGuire, M., Carroll, L. J., Yankie, L., Thrall, S. H., Dunaway-Mariano, D., Herzberg, O., Jayaram, B., and Haley, B. H. (1996) Determination of the nucleotide binding site within *Clostridium symbiosum* pyruvate phosphate dikinase by photoaffinity labeling, site-directed mutagenesis, and structural analysis, *Biochemistry 35*, 8544−8552.
15. Carroll, L. J., Xu, Y., Thrall, S. H., Martin, B. M., and Dunaway-Mariano, D. (1994) Substrate binding domains in pyruvate phosphate dikinase, *Biochemistry 33*, 1134−1142.
16. Otwinowski, Z., and Minor, W. (1997) Processing of X-ray diffraction data collected in oscillation mode, *Methods Enzymol. 276*, 307−326.
17. Storoni, L. C., McCoy, A. J., and Read, R. J. (2004) Likelihood-enhanced fast rotation functions, *Acta Crystallogr., D: Biol. Crystallogr. 60*, 432−438.
18. McCoy, A. J., Grosse-Kunstleve, R. W., Storoni, L. C., and Read, R. J. (2005) Likelihood-enhanced fast translation functions, *Acta Crystallogr. D: Biol. Crystallogr. 61*, 458−464.
19. Brunger, A. T., Adams, P. D., Clore, G. M., DeLano, W. L., Gros, P., Grosse-Kunstleve, R. W., Jiang, J. S., Kuszewski, J., Nilges, M., Pannu, N. S., Read, R. J., Rice, L. M., Simonson, T., and Warren, G. L. (1998) Crystallography & NMR system: a new software suite for macromolecular structure determination, *Acta Crystallogr. D: Biol. Crystallogr. 54*, 905−921.
20. Winn, M. D., Isupov, M. N., and Murshudov, G. N. (2001) Use of TLS parameters to model anisotropic displacements in macromolecular refinement, *Acta Crystallogr. D: Biol. Crystallogr. 57*, 122−133.
21. Jones, T. A. (2004) Interactive electron-density map interpretation: from INTER to O, *Acta Crystallogr. D: Biol. Crystallogr. 60*, 2115−2125.
22. Wei, M., Li, Z., Ye, D., Herzberg, O., and Dunaway-Mariano, D. (2000) Identification of domain-domain docking sites within *Clostridium symbiosum* pyruvate phosphate dikinase by amino acid replacement, *J. Biol. Chem. 275*, 41156−41165.
23. Navaza, J. (2001) Implementation of molecular replacement in AMoRe, *Acta Crystallogr. D: Biol. Crystallogr. 57*, 1367−1372.
24. McGuire, M., Huang, K., Kapadia, G., Herzberg, O., and Dunaway-Mariano, D. (1998) Location of the phosphate binding site within *Clostridium symbiosum* pyruvate phosphate dikinase, *Biochemistry 37*, 13463−13474.
25. Ye, D., Min, W., McGuire, M., Huang, K., Kapadia, G., Herzberg, O., Martin, B. M., and Dunaway-Mariano, D. (2001) Investigation of the catalytic site within the ATP-grasp domain of *Clostridium symbiosum* pyruvate phosphate dikinase, *J. Biol. Chem. 276*, 37630−37639.
26. Hayward, S., and Berendsen, H. J. (1998) Systematic analysis of domain motions in proteins from conformational change: new results on citrate synthase and T4 lysozyme, *Proteins: Struct., Funct., Genet. 30*, 144−154.
27. Cook, A. G., and Knowles, J. R. (1985) Phosphoenolpyruvate synthetase and pyruvate, orthophosphate dikinase: stereochemical consequences at both the β-phospho and γ-phospho groups of ATP, *Biochemistry 24*, 51−58.
28. Yankie, L., Xu, Y., and Dunaway-Mariano, D. (1995) Location of the catalytic site for phosphoenolpyruvate formation within the primary structure of *Clostridium symbiosum* pyruvate phosphate dikinase. 2. Site-directed mutagenesis of an essential arginine contained within an apparent P-loop, *Biochemistry 34*, 2188−2194.
29. Kraulis, P. J. (1991) A program to produce both detailed and schematic plots of protein structures, *J. Appl. Crystallogr. 24*, 946−950.
30. Bacon, D. J., and Anderson, W. F. (1988) A fast algorithm for rendering space-filling molecule pictures, *J. Mol. Graphics 6*, 219−220.
31. Merritt, E. A., and Bacon, D. J. (1997) Photorealistic molecular graphics, *Methods Enzymol. 277*, 505−524.

BI701848W